Replication defective viral genomes exploit a cellular pro-survival mechanism to establish viral persistence

Jie Xu[1,4], Yan Sun[1,4], Yize Li[2], Gordon Ruthel[1], Susan R. Weiss[2], Arjun Raj[3], Daniel Beiting[1], and Carolina B. López[1,*]

[1]Department of Pathobiology, School of Veterinary Medicine, University of Pennsylvania, Philadelphia, PA 19104, United States.

[2]Department of Microbiology, Perelman School of Medicine, University of Pennsylvania, Philadelphia, PA 19104, United States.

[3]Department of Bioengineering, School of Engineering, University of Pennsylvania, Philadelphia, PA 19104, United States.

[4]Authors contribute equally to this work.

***Corresponding author**: Carolina B. López, PhD. Department of Pathobiology, School of Veterinary Medicine, University of Pennsylvania, Philadelphia, PA 19104, United States

TEL 215-573-3493; Email lopezca@upenn.edu

Abstract Word Count: 147

Main Text Word Count: 3,847

ABSTRACT

Replication defective viral genomes (DVGs) generated during virus replication are the primary triggers of antiviral immunity in many infections. However, it is also well established that DVGs facilitate viral persistence. Why and how DVGs interact with the host to achieve these two opposing functions remains unknown. We report that DVGs engage a MAVS-mediated TNF response that selectively protects a subpopulation of cells from death and promotes the establishment of persistent infections. We find that this phenotype results from the dual activities of TNF, which drives apoptosis of highly infected cells while extending the survival of cells enriched in DVGs. The pro-survival effect of TNF depends on the activity of the TNFR2/TRAF1 pathway that is regulated by MAVS signaling. These results identify TNF as a pivotal factor in determining cell fate during a viral infection and delineate a MAVS/TNFR2-mediated mechanism that drives the persistence of otherwise acute viruses.

Keywords: Viral-host interactions, defective viral genomes, antiviral immunity, viral persistence, TNF signaling, paramyxovirus.

INTRODUCTION

Persistent viral genomes are observed after a number of acute viral infections in humans, including respiratory syncytial virus, measles, and Ebola [1-3]. A number of host factors, including impaired or altered cytokine production and progressive loss of immunological functions support the maintenance of persistent infections [4]. However, the processes and cellular mechanisms determining the onset of viral persistence after acute viral infections remain unknown.

The innate immune response is the first active host barrier to virus replication and is essential to control and clear the infection. The antiviral innate response is initiated upon recognition of viral molecular patterns by cellular sensor molecules. Activation of these sensor pathways leads to the expression of genes with pro-inflammatory, antiviral, and pro-apoptotic activities that control virus growth and spread. During infections with important human pathogens including the respiratory syncytial virus (RSV), parainfluenza virus, and measles virus, the antiviral response is triggered by replication defective copy-back viral genomes (DVGs) that accumulate during viral replication [5-8]. DVGs potently stimulate intracellular RIG-I-like receptors (RLRs) that signal through the mitochondrial antiviral-signaling (MAVS) protein to stimulate the expression of genes that control virus replication and spread, and direct clearance of infected cells [9,10].

Paradoxically, DVGs also promote the establishment of persistent RSV, parainfluenza, and measles virus infections in tissue culture [11-14] and are proposed to be responsible for establishing persistent Ebola virus infections in humans [1]. This pro-persistence activity of DVGs has been related to the continuous competition for the viral polymerase between full-length genomes and DVGs, resulting in alternating cycles of replication of full-length and defective

genomes [15-17]. However, this mechanism can't explain the survival of virus-infected cells in the presence of strong pro-apoptotic and antiviral molecules, including type I IFNs and TNFα, that are induced in response to sensing of DVGs [10].

In order to better understand the host-virus interactions driving the establishment of persistent infections of otherwise acute viruses, we developed technology that allowed us to investigate at a single cell level the mechanisms behind the different activities of DVGs in infected cells. Using fluorescent *in situ* hybridization targeting ribonucleic acid molecules (RNA FISH) to distinguish DVGs from standard viral genomes during infection, we reveal that DVGs from two different viruses accumulate only in a subpopulation of infected cells, and that these cells survive the infection longer than cells enriched in full-length virus, leading to the establishment of persistent infections. Moreover, the survival of DVG-high cells is dependent on MAVS signaling, and we identify TNFα produced in response to MAVS signaling as pivotal in determining cell fate. We show that while cells harboring full-length viral genomes die from virus induced TNF-mediated apoptosis, cells enriched in DVGs regulate the expression and activity of a TNFR2/TRAF1 pro-survival program that protects them from TNF-induced apoptosis. This study reveals a mechanism by which distinct viral genomic products determine cell fate upon infection by taking advantage of the dual functions of TNFα to perpetuate both virus and host.

RESULTS

DVGs dominate in a subpopulation of infected cells.

To better understand the impact of DVGs during infection, we established a RNA FISH assay that allowed us to differentiate full-length genomes from the murine parainfluenza virus Sendai (FL-gSeV) from SeV DVGs at a single cell level. As copy-back DVGs are generated from the 5'end of the viral genome and thus have a high sequence homology with the FL-gSeV [18,19], we utilized a two-color probing strategy to distinguish DVGs from FL genomes within infected cells (Figure 1A). To detect replicating virus, a set of probes labeled with Quasar-570 (pseudo-colored red) was designed against the 5' end of the positive sense viral RNA and a different set of probes labeled with Quasar-670 (pseudo-colored green) was designed against the 3' end of the positive sense SeV genome, which covers the viral genomic sequence shared with DVGs. As a result of this design, DVGs are only bound by Quasar-670-labeled probes (denoted 'DVG'), while FL-gSeV are bound by a combination of Quasar-570 and Quasar-670-labeled probes (denoted 'FL-gSeV' and appearing as orange in the images) (Figure 1A). To test the specificity of the labeling, we infected cells with SeV lacking DVGs (LD) alone or complemented with purified defective particles containing DVGs (pDPs). Cells infected with SeV LD demonstrated a strong FL-gSeV signal and no DVG signal, while addition of pDPs resulted in detection of cells with strong positive DVG signal (Figure 1B). Further, Quasar-670-labeled DVG probes detected *in vitro* transcribed DVG RNA transfected into cells and did not cross-react with the synthetic RNA poly I:C or with host GAPDH mRNA (Figure 1C and S1A and B), confirming their specificity.

Analysis of various epithelial cell lines infected with SeV containing high levels of DVGs (HD) showed an unexpected heterogeneous distribution of Quasar-570 and 670 signals at 24 and 48 h post infection, indicating differential accumulation of DVGs and FL-gSeV among infected cells (Figure 1D and Figure S1C). The phenotype was recapitulated upon hybridization

with probes that targeted the negative sense FL-gSeV (Figure S1D). In addition, heterogeneous distribution of FL-gSeV and DVGs was also observed upon natural accumulation of DVGs *in vivo* during SeV infection (Figure 1E). Further, after sorting cells negative for both Quasar-570 and 670 staining (Non-detected: ND, gated in blue), DVG-high (gated in green), and FL-gSeV high (FL-high, gated in orange), we confirmed their differential content of FL-gSeV and DVG by RT-qPCR (Figures 1F-H). An intermediate cell population showing strong Quasar-670 signal and positive for Quasar-570 (INT, gated in yellow) was also observed by flow cytometry (Figures 1F and G). This population demonstrated moderate levels of SeV NP transcript, moderate FL-gSeV, and relatively high levels of DVGs by RT-qPCR (Figure 1H and not shown). Because of its intermediate nature, we excluded this population from further analysis in this study.

To characterize the temporal distribution of DVGs among the infected cell population, we analyzed cells infected with SeV HD by RNA FISH followed by flow cytometry. FL-high and DVG-high cells were detected as early as 6 h post infection and their percentage increased during the time course of infection, corresponding well with cell imaging (Figures 1I and J). DVG-high cells accumulated quickly upon infection, plateaued, and decreased at later time points, while accumulation of FL-high cells followed behind, reminiscent of the waves of accumulation of defective interfering particles and FL-genomes used to explain the interfering activity of DVGs (Figure 1K) [20,21]. As expected based on their characterization of primary immunostimulatory molecules during SeV infection [9,10,22], early accumulation of DVG-high cells was associated with expression of high levels of *IFNB1* mRNA (Figure 1L). In contrast, the kinetics of SeV NP mRNA expression followed that of the FL-high populations, but not that of

the DVG-high population. Taken together, these data demonstrate a heterogeneous physical and functional distribution of DVGs and FL-gSeV during SeV infection.

DVG-high cells are less prone to apoptosis than FL-high cells, facilitating the development of persistently infected cultures.

To examine how DVG accumulation in a subpopulation of cells impact the establishment of persistently infected cultures, we infected susceptible LLC-MK2 cells with SeV LD or HD and monitored the presence of infected cells overtime. Cultures infected with SeV LD died 8 days after infection (Figures 2A and B), while cultures infected with SeV HD recovered from a cell death crisis and were able to be passaged for at least 17 days (Figures 2A, 2B and S2A). Remarkably, a substantially higher proportion of DVG-high cells survived by day 5 post SeV HD infection compared to FL-high cells (Figure 2A), and by day 17 post infection, approximately 34% of the total survivors were DVG-high compared to 5.47% FL-high (Figure 2C). Importantly, infectious virus was detected in the supernatant of survivor cells at day 17 post SeV HD infection, confirming the ability of DVGs to support a persistent productive infection (Figure 2D). The predominance of DVG-high cell in the surviving cell population together with our inability to generate persistently infected LLC-MK2 cultures during infection with SeV LD virus stocks, suggest that DVGs confer resistance to SeV-induced cell death. In support, the percentage of dead cells measured by viability staining was significantly higher in FL-high cells than DVG-high cells at 24 and 48 h post infection in both LLC-MK2 and A549 cells (Figure 2E and F, and data not shown). Notably, the percentage of dead cells among the DVG-high sub-population did not significantly increase over time, whereas the percentage of dead cells among FL-high cells increased at 48 h post infection matching the spike on total cell death in the culture

(Figure 2G). To assess whether DVGs protect cells from apoptosis, a major mechanism of cell death during SeV infection [23,24], we stained the cultures for the hallmark apoptotic molecules active caspase 3 and cleaved PARP. A significantly smaller population of DVG-high cells stained positive for active-caspase 3 or cleaved-PARP protein compared to FL-high cells (Figures 2H and I, and S2B) demonstrating that DVGs protect cells from apoptosis during infection.

To investigate whether the differential accumulation of DVGs and FL-genomes among infected cells and the associated phenotype applied to other paramyxoviruses, we infected A549 cells with RSV with a high content of DVGs (HD) and analyzed the cultures by RNA FISH using specific probes designed following the same strategy as described for SeV. As with SeV HD infection, heterogeneous accumulation of RSV DVGs and full-length RSV genomes (FL-gRSV) was observed in the infected culture (Figures 3A and B). Similarly to SeV infection, cells infected with RSV LD did not generate distinguishable DVG signal (Figure 3C). In addition, infection with RSV HD resulted in a persistently infected culture with survivor cells containing substantial amount of both FL-gRSV and DVGs (Figures 3C and S3), while cells infected with RSV LD died after one week of infection (Figure 3C and D). Further, DVG-high cells were protected from virus-induced cell death, as the percentage of apoptotic cells stained for active-caspase 3 was significantly lower in DVG-high cells compared to FL-high cells (Figure 3E and F). Taken together, DVG-high cells are less prone to apoptosis than FL-high cells during SeV and RSV infection and extended cell survival associates with the establishment of persistent infections.

DVG-high cells express a unique transcriptional profile enriched in genes encoding pro-survival proteins.

To characterize the mechanism protecting DVG-high cells from apoptosis, we identified candidate pathways by transcriptionally profiling sorted FISH-stained ND, FL-high, and DVG-high cells at 24 h post SeV HD infection using RNA-Seq. A detailed description of the pipeline for these studies is presented in Figure S4A. Sorted populations with higher than 90 % purity from multiple independent experiments were pooled after RNA extraction and used for total transcriptome profiling (Figures S4B and C). Confirming the distribution of viral genomes in the different populations, RNA-Seq analysis demonstrated even coverage of the full length genome in the FL-high population, while showing a strong bias towards the 5' end of the genome in the DVG-high population, as expected based on the origin of SeV DVGs [18,22] (Figure S4D).

RNA-Seq analysis identified 1800 differentially expressed genes among the FL-high, DVG-high, and ND populations (≥ 2 fold change in expression with ≤ 1% false discovery rate). Increased expression of a number of genes in the different cell populations was validated by RT-qPCR (Figure S4E). Hierarchical clustering revealed at least three distinct clusters of co-regulated genes. Clusters 1, 2, and 3 represent genes with relatively higher expression in ND cells, DVG-high cells, or FL-high cells, respectively (Figure 4A). Gene Ontology analysis of cluster 1 (upregulated in ND cells) was highly enriched in genes involved in cell cycle checkpoints, complement and antigen presentation, and the IFN signaling pathway (Figure 4B). Cluster 3 (upregulated in FL-high cells) showed enrichment in genes involved in the unfolded protein responses, oxidation-reduction pathways, and steroid metabolism (Figure 4B). Cluster 2 (upregulated in DVG-high cells) demonstrated the enrichment of anti-apoptotic factors and a number of pro-survival pathways, including mitogens and growth factors, the TNF pathway, and

the NF-kB/Rel pathway (Figure 4B). Gene set enrichment analysis (GSEA) confirmed enriched signatures associated with pro-survival pathways in the DVG-high population (Figures 4C-D). These signatures include TNF-related genes with anti-apoptotic functions, such as the TNF receptor 2 (*TNFR2* or *TNFRSF1B*), TNF receptor associated factor 1 (*TRAF1*), and the TNF alpha induced protein 3 (*TNFAIP3*, also known as A20) [25], molecules involved in regulation of NF-κB activity (for example, *NFKBIA* and *NFKBIE*) [26], and a number of genes involved in apoptosis regulation, including the baculoviral IAP repeat containing 3 (*BIRC3*, also know as c-IAP2) [27,28] (Figure 4D). In addition, the DVG-high population was enriched in genes involved in the induction of IFNs and expression of cytokines and chemokines, consistent with a well-described role of DVGs in initiating antiviral immunity [9,10,29]. Collectively, these studies show that host cells enriched in DVGs actively engage both an anti-viral and a pro-survival program.

DVG-high cells are protected from a MAVS/TNF-dependent apoptosis.

To determine if accumulation of DVG-high cells and death of FL-high cells depended on the antiviral response induced by DVGs [9,10], we analyzed infections of cells lacking the critical adaptor protein MAVS (MAVS KO) or lacking the type I IFN receptor (IFNAR1 KO). In this setting, differential accumulation of DVG-high and FL-high cells remained unchanged in MAVS or IFNAR1 KO cells, suggesting that the heterogeneous accumulation of DVGs is independent of the engagement of the antiviral response (Figure 5A). In addition, the percentage of apoptotic cells in both DVG-high and FL-high populations, remained similar in WT and IFNAR1 KO cells (Figures 5A-C). In contrast, MAVS KO cells exhibited reduced apoptosis in both subpopulations (Figure 5A-C), indicating that a MAVS-dependent process drives apoptosis in these cultures. The lower level of apoptosis in SeV HD infected MAVS KO cells compared to controls was not

due to reduced viral replication, as MAVS KO cells showed increased viral replication (Figure S5A).

Transcriptional profiling suggested that TNFα-related pathways are implicated in defining the cell fate during SeV infection. Due to the well-documented dual roles of TNFα in both inducing cell death and conferring survival [30], we next investigated whether TNFα signaling orchestrates the differential pro- and anti-apoptotic responses of FL-high and DVG-high cells. As expected, SeV infection induced high levels of TNFα protein and mRNA in a MAVS-dependent but IFNAR1-independent manner (Figure 5D and Figure S5B). The absence of TNFα secretion in MAVS KO cells correlated with their decreased level of apoptosis in response to SeV infection (Figures 5A and B), and supplementation of MAVS KO cells with TNFα, but not IFNβ, significantly increased apoptosis upon infection with SeV HD (Figure 5E) or LD (Figures S5C and D). Moreover, a combination of neutralizing antibodies against TNFα and its receptors significantly reduced the level of total active-caspase 3 expression (Figures 5F and S5E), indicating a role of the MAVS/TNF axis in regulating cell death in these cultures. To investigate whether TNFα differentially impact apoptosis of FL-high and DVG-high cells, we quantified the percentage of active caspase-3 positive cells among each sub-population during infection in the presence of neutralizing antibodies. Unexpectedly, blocking TNFα signaling reduced apoptosis of FL-high cells while increased apoptosis of DVG-high cells, suggesting that TNFα signaling protects DVG-high cells while killed FL-high cells (Figure 5G). Interestingly, supplementation of MAVS KO cells with increasing doses of TNFα enhanced apoptosis in the infected culture (Figure 5G and H), but did not phenocopy the differential effect on cell death of FL-high and DVG-high cells seen in WT infected cells, as both sub-populations were susceptible to TNFα-induced apoptosis to a similar extent at all doses tested (Figure 5H and I). Taken together, these

results suggest that DVG-high cells lose protection from TNFα mediated apoptosis in absence of MAVS and suggest a direct role of MAVS signaling in promoting the survival of DVG-high cells.

MAVS signaling dictates the survival of DVG-high cells.

We next investigated how DVG-high cells become less prone to TNFα-mediated apoptosis compared to FL-high cells within the same infected culture. Based on RNA-Seq data showing upregulation of several genes in the TNFR2 signaling pathway in DVG-high cells, including TNFR2 itself (*TNFRSF1B*) and *TRAF1*, we hypothesized that the TNFR2 pathway is responsible for the protection of DVG-high cells from virus-triggered apoptosis. To test this hypothesis, we neutralized either the primary TNF receptor, TNFR1, or TNFR2 in SeV HD infected cultures (Figures 6A and B) and tested for apoptosis of the different sub-populations. Treatment with TNFR2 neutralizing antibodies significantly increased apoptosis of DVG-high but not FL-high cells, suggesting a pro-survival function of TNFR2 signaling in cells enriched in DVGs. In contrast, blocking TNFR1 signaling reduced cell death in FL-high but had no impact on the survival of the DVG-high population (Figures 6A and B) suggesting that TNFR1 signaling is not necessary for DVG-survival. In agreement with a pro-survival role for TNFR2 in DVG-high cells, knockdown of the TNFR2 adaptor molecule TRAF1 increased the level of apoptosis only in DVG-high but not in FL-high cells (Figures 6C-D and S6). Interestingly, DVG mediated upregulation of TNFR2 signaling was controlled by MAVS, as MAVS KO cells showed impaired upregulation of surface TNFR2 expression and blunted expression of the pro-survival genes *TRAF1*, *BIRC3*, and *TNFAIP3* upon infection with SeV HD (Figure 6E and F). Thus, the TNFR2 pathway, which is upregulated in DVG-high cells in a MAVS-dependent

manner, protects this population from SeV induced TNFα mediated apoptosis. Together, these data demonstrate that engagement of MAVS/TNFR2 axis by DVGs allow a sub-population of infected cells to survive TNFα mediated apoptosis, which is potentially exploited by the virus to achieve long-term persistence.

DISCUSSION

In this study we demonstrate that while cells respond to DVGs inducing the expression of anti-viral molecules that restrict virus production, they also engage a pro-survival TNFR2/TRAF1-dependent mechanism that promotes viral persistence. Our data support a model in which enrichment of DVGs over full-length viral genomes in infected cells leads to the strong engagement of a MAVS-dependent pathway that while driving anti-viral and pro-apoptotic activities through the production of IFNs and TNFα, protects the cytokine-producing cell from death by inducing and engaging TNF-related pro-survival factors (Figure 6G). These observations not only explain a long-standing paradox between the reported immunostimulatory and pro-persistence activities of DVGs, but also reveal complex host-pathogen interactions that may, in part, explain the co-existence of viruses and their hosts in immunocompetent individuals.

The testing and validation of this model was only possible after developing the ability to identify and distinguish DVGs from FL-genomes at a single cell level. Prior to our imaging approach, DVGs could only be detected PCR or northern-blot in bulk infected cultures, masking the heterogeneity of viral genome distribution among infected cells, as well as the distinct cellular responses towards the infection. Of note, in A549 and LLC-MK2 cells the DVG signal was widely spread within the cell cytoplasm, while the FL-gSeV signal was concentrated in a perinuclear region of the infected cells (Figures 1D and J) indicating a differential intracellular

localization for FL-gSeV and DVGs. In agreement, in cells infected with SeV lacking DVGs (SeV LD), FL-gSeVs were concentrated in the perinuclear region (Figure 2A and S1A). The impact of the intracellular distribution of viral genomes is unknown and is currently under investigation.

Our DVG specific RNA FISH revealed two phenomena that challenge the prevailing view of the temporal and spatial dynamics of DVGs during infection and provide new insights into their contribution to virus persistence. First, instead of a homogenous distribution of DVGs together with FL-viral genomes among infected cells, DVGs predominantly occupied a sub-population of the infected cells. Second, changes in the percentage of DVG-high cells throughout the course of infection coordinated well with changes in the percentage of FL-high cells, providing an alternative explanation for the long standing observation of waves of DVGs and FL-viral genome dominance in infected cultures [16,31]. Our evidence of distinct cellular populations based on viral genomic content and the resulting differential susceptibility to cell death, reveal an underappreciated cellular level of regulation of persistent viral infections.

Our data demonstrate that, during virus infection, cells with a high content of FL-gSeV are susceptible to TNFα but not type-I IFN mediated apoptosis. The apparent lack of pro-apoptotic activity of IFN over FL-high cells is likely caused by the strong IFN signaling antagonistic activity of paramyxovirus proteins [32]. TNFα is a pro-inflammatory cytokine that can be induced by viral infection and plays important roles in the control of virus dissemination [33,34]. Expression of TNFα has been reported in many paramyxovirus infections, including RSV, SeV, Newcastle disease viruses, and parainfluenza virus 5 (also known as simian virus 5) [35,36]. Importantly, TNFα expression is stimulated by DVGs in both SeV and RSV infections [6,29]. In addition, purified defective viral particles from SeV can cause selective apoptosis of transformed

cells by activating the TNF-related apoptosis-inducing ligand (TRAIL) both *in vitro* and *in vivo* [37]. Together, this evidence indicates that DVGs can drive TNF-mediated apoptosis of virus infected cells through a mechanism distinct from that leading to cell death after LD infections, likely caused by virus induced cell stress.

Unexpectedly, a robust pro-survival TNF signature was found in DVG-high cells. Further, neutralization of TNFα and its receptors during SeV infection resulted in significantly increased apoptosis of DVG-high cells, confirming a critical requirement for cell extrinsic TNF signaling in promoting the survival of these cells. The enhanced survival of DVG-high cells compared to FL-high cells could be explained also by reduced lytic virus replication (and viral protein expression) in DVG-high cells as DVGs interfere with the replication of the FL-gSeV by competing for the usage of the viral polymerase [16,17]. However, both SeV and RSV-induced apoptosis were significantly reduced in MAVS KO cells compared to control cells despite similar or even higher levels of replication in MAVS KO, indicating that death is not primarily a result of virus replication. The pro-survival response to TNFα signaling is a well-documented protective mechanism mediated by NF-kB induced upregulation of pro-survival molecules, including TRAF1, A20 (*TNFAIP3*) and cIAP2 (*BIRC3*) [38-41]. Here we identified a TNFR2/TRAF1 mediated pathway as essential to the survival of DVG-high but not FL-high cells. Notably, the expression and activity of key elements in this pathway, including TNFR2 and TRAF1, required the engagement of MAVS signaling in DVG-high cells. In the absence of MAVS, TNFα treatment rendered DVG-high and FL-high cells equally susceptible to apoptosis. This discovery uncouples the role of the TNF pathway in dictating the individual cell fate during infection and identifies the interaction of DVGs with the MAVS-mediated antiviral pathway as a critical factor in defining cell survival upon infection. The existence of a subset of pro-survival

oriented infected cells likely represents an evolutionary advantage of DVGs to the virus by maintaining a reservoir of FL-viral genomes.

Overall, here we describe an intricate mechanism in which virus and host come to a balance to establish a symbiotic interaction. The virus benefits from this mechanism because it allows extended survival of virus-infected cells, establishing a persistent infection. This relationship is founded in the dual role of TNF in targeting highly infected cells (FL-high) for apoptosis while protecting cells with active MAVS signaling (DVG-high) from cell death. This mechanism fundamentally changes our understanding of the relationship between antiviral responses and viral persistence and reveals potential therapeutic targets to eliminate persistent viral reservoirs.

METHODS

Ethics statement.

Studies in mice were carried out in strict accordance with the recommendation in the Guide for the Care and Use of laboratory Animal of the National Institute of Health. The protocol (804794) was approved by the Institutional Animal Care and Use Committee, University of Pennsylvania Animal Welfare Assurance Number A3079-01.

Cell cultures and stable cell lines.

A549 cells (human type II alveolar cells, ATCC, #CRM-CCL185), LLC-MK2 (monkey kidney epithelial cells, ATCC, #CCL-7), and control, MAVS KO, IFNAR1 KO A549s were cultured at 5% CO_2 and 37°C conditions with Dulbecco's modified Eagle's medium supplemented with

10% fetal bovine serum, 1 mM sodium pyruvate, 2 mM L-Glutamine, and 50 mg/ml gentamicin. All cell lines were treated with mycoplasma removal agent (MP Biomedicals) and routinely tested for mycoplasma before use. KO A549 cells were generated using CRISPR/Cas9 as follows: The oligonucleotide sequences sgMAVS-for: CACCGGAGGGCTGCCAGGTCAGAGG and sgMAVS-rev**:**AAACCCTCTGACCTGGCAGCCCTC (IDT) ; sgIFNAR1 (set 1) for: CACCGGACCCTAGTTGCTCGTCGCCG and sgIFNAR1 rev: AAACCGGCGACGAGCAACTAGGGTC; sgIFNAR1 (set 2) for: CACCGTGGGTGTTGTCCGCAGCCGC and sgIFNAR1 rev: AAACGCGGCTGCGGACAACACCCA (Invitrogen) were used for generation of single guide RNAs (sgRNA) to target MAVS or IFNAR1 genes. The forward and reverse oligonucleotides were inserted into the plasmid vector pLenti-CRISPR(Addgene) using BsmBI restriction sites. The resulting plasmids were packaged in pseudo lentiviral particles and used to establish the gene KO as previously described [42]. KO of MAVS was confirmed by western blotting and mutations in the gene were verified by PCR using the following primers: MAVS-For: CTCCCCTGGCTCCTGTGCTCC and MAVS-Rev: AACTCCCTTTATTCCCACCTTG. KO of IFNAR1 was confirmed by flow cytometry after IFNα treatment of cells and mutations were verified by PCR using the primers IFNAR1-For: GCTAGCTAGGAGGAAAGGCG and IFNAR1-Rev: GGGTTTAATCTTTGGCGCGG.

Mice experiments.

C57BL/6 mice were obtained from Taconic Farms, Inc. Female mice of 6-8 weeks of age were used. All mice were housed in pathogen-free mouse facility. For SeV infection, mice were

anesthetized with Ketamine HCl (Ketaset) and Xylazine (LLOYD Laboratories) and inoculated intranasally with 35 µl of PBS containing 10^4 $TCID_{50}$ of SeV. After 5 days of infection, mice were sacrificed and their lungs were inflated and preserved in O.C.T. compound (Sakura Finetek) diluted in PBS (3:2 ratio) for RNA FISH imaging.

Viruses.

Sendai virus strain 52**,** Sendai virus strain Cantell HD and LD stocks (SeV HD, high DVG particle content; SeV LD, low DVG particle content) were prepared in embryonated chicken eggs as described previously [9,10]. SeV Cantell HD stock had consistently an infectious: total particle ratio of 5,00-15,000. RSV-LD (stock of RSV derived from strain A2, ATCC, #VR-1540 with a low content of DVGs) and RSV-HD (stock of RSV derived from strain A2, ATCC, #VR-1540 with a high content of DVGs) were prepared and characterized as described previously [6,43]. For SeV titration, LLC-MK2 cells were infected with triplicate serial 1:10 dilutions of the virus stock or 1:10 dilution of supernatant from infected cell cultures in the presence of 2 mg/ml of trypsin to determine the medium tissue culture infectious dose ($TCID_{50}$). After 72 h of incubation at 37°C, supernatant from each well was tested by hemagglutination of chicken RBCs for the presence of virus particles at the end point dilution as describe in [9]. For virus infections *in vitro*, cells were incubated with virus at a multiplicity of infection (MOI) of 1.5 $TCID_{50}$/cell unless otherwise indicated in the figure.

RNA extraction and RT-qPCR.

Total RNA was extracted using TRIzol (Invitrogen) according to the manufacturer's specifications and 1-2 µg of RNA was reverse transcribed using the High Capacity RNA-to

cDNA kit (Applied Biosystems). cDNA was amplified with specific primers in the presence of SYBR green (Applied Biosystem). qPCR reactions were performed in triplicate using an Applied Biosystem ViiA7 Real-time Lightcycler. For the primers used, see Table S1. For FL-gSeV and SeV DVGs detection 1-2 µg of isolated total RNA was reverse transcribed with specific primers for DVG (5'GGTGAGGAATCTATACGTTATAC3') and FL-gSeV (5'-TGTTCTTACTAGGACAAG-3') using Superscript III without RNaseH activity to avoid self-priming. Recombinant RNase H (Invitrogen) was later added to the reverse transcribed samples. cDNA was amplified with viral product specific qPCR primers listed in Table S1 in the presence of SYBR green (Applied Biosystem). Copy numbers were normalized to the housekeeping gene *GAPDH*. RSV DVGs were detected by regular PCR method. Detailed PCR conditions for RSV DVGs and genome detection can be found in previous publications of the lab [6].

Preparation of *in vitro* transcribed DVG RNA.

To generate *in vitro* transcribed SeV DVG RNA, a plasmid expressing SeV-DVG (pSL1180-DVG546 described previously in Xu et al., 2015), was linearized and *in vitro* transcribed using the MEGAscript T7 kit (Ambion) in the presence of RNase inhibitors (Invitrogen). The resulting products were then treated with DNase and then precipitated with LiCl (both included in the MEGAscript T7 kit). All *in vitro* transcribed DVG RNA had optical density at 260 nm (OD260)/ OD280 ratios between 2.00 and 2.25, and the OD260/ OD230 ratios were between 2.20 and 2.60.

Single-molecule RNA fluorescence *in situ* hybridization (RNA FISH) and immunofluorescence staining (IF).

RNA fluorescence *in situ* hybridization (RNA FISH) was performed according to published protocols with some modifications [44]. The probes used for both SeV and RSV detection were single stranded DNA oligos (20 nucleotides) each labeled with one fluorophore (Quasar 570 or Quasar 670, Biosearch Technologies). Briefly, probes detecting positive sense FL-gSeV genome and most viral mRNA targeted position 1 to 11630 of the SeV genome (excluding the 5' end that encompasses the DVG sequences) and labeled with Quasar 570; probes detecting positive sense DVGs were labeled targeted position 14965 to 15416 of the SeV genome and were labeled with Quasar 670. For detecting negative sense FL-gSeV, a pool of Quasar-570 labeled probes target position 1 to 14435 of the negative sense FL-gSeV was used. For RSV FISH probes: a pool of 32 probes detecting positive sense FL-gRSV genome were designed targeting from position 1 to 11929 of the RSV genome (excluding the 5' end that encompasses the RSV DVG sequences) and labeled with Quasar 570; probes detecting positive sense copy-back RSV DVGs targeted position 14925 to 15225 of the RSV genome and were labeled with Quasar 670. For RNA FISH, cells were plated onto coverslips (Corning) at a density of 4×10^5 cells/well in 6-well plates and grown overnight at 37°C. The cells were washed once with ice-cold PBS followed by fixation with 4 % formaldehyde in PBS for 10 mins and then permeabilized in 70 % ethanol. Fixed cells were then equilibrated in wash buffer containing 10 % formamide and 2X saline sodium citrate (SSC [1X SSC is 0.15 M NaCl plus 0.015 M sodium citrate], all from Thermo Fisher Scientific). RNA FISH was performed by hybridizing fixed cells with probes (125 nM for SeV and 250 nM for RSV for *in vitro* samples, and 1.25 μM for *in vivo* SeV samples) diluted in 50 μl hybridization buffer consisting of 10 % formamide, 2X SSC, and 10% (wt/vol) dextran sulfate. Hybridization was performed overnight in a humidified chamber at 37°C. Nuclear staining using 0.5 μg/ml of Hoechst 33342 (Invitrogen) was performed afterwards and the coverslides were

mounted in GLOX anti-fade media (10 % glucose, 1M Tris-HCL pH8.0, glucose oxidase, catalase, diluted in 2X SSC; all from Sigma) before imaging. For RNA FISH coupled with IF (RNA FISH-IF), fixed cells were permeabilized with 70 % ethanol for 1 h. Permeabilized cells were then incubated with anti-human active-caspase 3 antibody (1:100 dilution; Cell Signaling) or anti-human cleaved-PARP antibody (1:100 dilution; Cell Signaling) followed by Alexa Fluor 488- labeled goat anti-rabbit IgG (1:500 dilution; Invitrogen) diluted in 1% BSA in the presence of 40 U/ml RNase inhibitor (Invitrogen). Stained cells were incubated in 4 % formaldehyde for 10 min prior to RNA FISH, washed with PBS, and then equilibrated in wash buffer. RNA FISH was then performed as described above. Imaging acquisition was performed with a Nikon E600 epifluorescence microscope equipped with a 20X, 40X and a 100X-1.4 numerical aperture oil immersion objective (Zeiss) and a Zeiss AxioCam MRm camera. **Bright field** image acquisition was performed on an Olympus CKX41 inverted microscope equipped with a 20X objective and a Spot Idea 5 MP Scientific Digital camera system (Diagnostic Instrument).

Image analysis and quantification.

Image analysis and quantification was performed using the Meta-morph software (Molecular Devices). Exposure time, gain, and offset were held constant for all images. The Multi-wavelength cell scoring module was applied to determine average fluorescent intensity of Quasar 570, Quasar 670 probe signals or targeted host protein signals in each cell. Pixel brightness of the signals in multiple empty areas of each images were used as a reference to set the threshold for positive staining of probe/antibodies. Because of the bi-color FISH probe design strategy for distinguishing DVG from FL-gSeV, each individual cell was quantified for their viral RNA content as a ratio of Quasar 670 versus Quasar 570 probe signal fluorescent intensity

(gSeV/DVG or gRSV/DVG). For image quantification of SeV infected cells (gSeV staining positive), a ratio below 0.8 was considered as FL-high cells, between 0.8-1.0 as intermediate (INT) and above 1.0 as DVG-high. For image quantification of RSV infected cells (RSV staining positive): a ratio below 0.5 was considered as FL-high cells, between 0.5-0.8 as intermediate (INT) and above 0.8 as DVG-high. For quantifying FISH coupled with active-caspase 3 staining images, same threshold value of gSeV/DVG or gRSV/DVG ratio was used to categorize cells into FL-high or DVG-high sub-population. Active-caspase 3 positive and negative cells were identified by positive scoring using a set threshold for positive staining and then the percentage of active-caspase 3 positive cells from FL-high and DVG-high cells was calculated. All images shown were quantified from at least 500 cells from four different fields in each repeat through at least three independently repeated experiments.

RNA FISH-FLOW and FACS-sorting.

The same procedure was applied for RNA FISH-FLOW cytometry (RNA FISH-FLOW) as was used for the slides based RNA FISH described previously excepted that cells were kept in suspension throughout the staining process. Briefly, monolayer cells were trypsinized, resuspended in 1% FBS in PBS, then fixed and permeabilized in 100% methanol for at least 15 min on ice. Hybridization was performed in100 µl hybridization buffer in presence of 1.25 µM RNA FISH probes for 16 h in a humidified chamber at 37°C. Cells were suspended in GLOX anti-fade media before flow cytometry/FACS. For live/dead staining (L/D Aqua), trypsinized cells were incubated with efluor-506 fixable viability dye (L/D Aqua, eBioscience) diluted in 1% FBS/PBS in the presence of 40 U/ml RNase inhibitor (Invitrogen) prior to fixation. Data was acquired in a BD LSRFortessa™ equipment (filter 582/15-Green for the detection of Quasar

570-gSeV probe; 670/30-Red for the detection of Quasar 670-DVG probe; 515/30-Blue for the detection of L/D staining). A BD FACSAria II machine was used for sorting RNA FISH probe hybridized A549 cells infected with SeV HD for 24h. Sorted cells (≥90% purity from parental gate) were centrifuged and preserved in TRIzol (Invitrogen) for RNA extraction and RNA-Seq analysis. Flow cytometry data analysis was performed using BD FACSDiva (BD Bioscience) or FlowJo (Tree Star) softwares.

RNA-Seq of FISH FACS-sorted cells.

Four sub-populations of cells (ND, FL-high, DVG-high and INT) were sorted from infected cultures after RNA FISH. RNA-Seq was performed in two replicates where the RNA of each replicate was a pool from 3 independent FISH-FACS sortings (6 independent sortings in total). RNA samples from FISH-FACS-sorted cells were prepared as follows: RNA extracted using TRIzol reagent was re-purified using the PicoPure™ RNA isolation kit (Thermo Fisher Scientific). Quality of the RNA was assessed by using the RNA Pico 6000 module on an Agilent Tapestation 2100 (Agilent Technologies). A schematic diagram for the FISH-FACS-sorting pipeline coupled with RNA-Seq is provided in Fig. S5A. Briefly, total cDNA libraries were prepared starting from 75 ng of extracted raw RNA using the Illumina TruSeq Stranded Total RNA LT kit with Ribo-Zero Gold, according to the manufacturer's instructions. Samples were run on Illumina NextSeq 500 to generate 75 bp, single-end reads, resulting in 21-53 million reads/sample with an average Q30 score ≥ 96.8%. All data were processed and analyzed by R programming language (v 3.2.2, R core team, 2016) and the RStudio interface (v 0.99.489), as described previously [45]. For host transcriptome analysis, raw fastq files were mapped to the human transcriptome (cDNA; Ensembl release 86) using Kallisto with 60 bootstraps per sample

[45,46]. Annotation and summarization of transcripts to genes was carried out in R, using the TxImport package[47]. Differentially expressed genes (≥ 2 fold and ≤ 1% false discovery rate) were identified by linear modeling and Bayesian statistics using the VOOM function in Limma package [48,49]. Gene Ontology (GO) was performed using the Database for Annotation, Visualization and Integration of Data (DAVID) [50,51]. Gene Set Enrichment Analysis (GSEA) was analyzed through Molecular Signatures Database (MSigDB) using the C2 canonical pathway collection [52]. For genome alignment, seq reads from the duplication of each population were combined and aligned to the full length genome of SeV strain Cantell using Subread aligner in the RSubread package [53]. This allowed us to extract only the viral reads from the total. Resulting BAM files were visualized as a track on the full length SeV Cantell genome using the Genious software (version 7.1.9, Biomatters develop team) for further alignment to the full length SeV Cantell genome to obtain the different coverages of viral reads from each of the four populations.

TNFR2 extracellular staining for flow cytometry

Extracellular staining of TNFR2 on A549 cells for flow cytometry was performed as follows: cells harvested in 1% FBS PBS were stained with anti-human-TNFR2 antibodies (2 μg/10^6 cells, R&D system) in 1% FBS PBS on ice for 40 min, washed three times by 1%FBS PBS and then subjected to secondary antibody staining using goat anti-donkey Alexa Fluor 488 antibody (Invitrogen;1:1000 diluted in 1%FBS PBS) on ice for 30 min. Stained cells was acquired in a BD LSRFortessa™ and analyzed using the FlowJo (Tree Star) software.

TNFα neutralization and supplementation of infected cells.

For TNFα neutralization experiments, 70-80 % confluent A549 cells were pre-treated with neutralizing antibody against control IgG or TNFα, TNFR1 and TNFR2 (R&D system) at 2 μg/ml/antibody or with IgG control antibody (R&D system) at the same concentration diluted in 400 μl of DMEM-2% FBS culture media. After 3 h, pre-treated cells were infected with SeV HD at an MOI of 1.5 diluted in 100 μl of the same media. Samples were collected after 20 and 30 h post infection for analysis. For TNFα supplementation experiments, human recombinant TNFα (Peprotech) was added to the media of infected cells at the indicated doses after 16 h of SeV HD infection. Sample were collected 8 h post treatment for further analysis.

RNA interference.

siRNAs for human *TRAF1* (ON-TARGET plus smart pool, 7185, including 4 target sequences: GAAGGACGACACAAUGUUC, GAACUCAGGAGAAGGCUCA, GGAAAGAGAACCCAUCUGU, UGUGGAAGAUCACCAAUGU) and ON-TARGET plus non-targeting control pool were obtained from GE health, Dharmacon. Briefly, 3 x 10^4 A549 cells were transfected with 50 μM of siRNAs using Lipofectamine RNAiMAX transfection reagent (Invitrogen) according to the manufacture's protocol. After 16 h of incubation, media was replaced with complete cell culture media without antibiotics. After 40 h of transfection, cells were infected with SeV HD (MOI= 1.5 $TCID_{50}$/cell) for 24 h. Cells were harvested with TRIzol for RNA preparations, NP-40 lysis buffer for protein preparations, or treated with 4% formaldehyde for image analysis. As control, cells were treated with equal amount of non-targeting scramble siRNA using Lipofectamine RNAiMAX transfection reagent (Invitrogen) as used in siRNA assay.

Statistical analysis

All statistical analyses were performed with GraphPad Prism version 5.0 (GraphPad Software, San Diego, CA). A statistically significant difference was defined as a p value if <0.05 by either one-way or two-way analysis of variance (ANOVA), significance of variance (F value), or Student's t with or without a *post hoc* test to correct for multiple comparisons on the basis of specific data sets as indicated in each Figure legend.

Data availability

All data are available upon request to the corresponding author. Raw RNA-Seq data of FISH-FACS sorted cells have been deposited on the Gene Expression Omnibus (GEO) database for public access (GSE96774).

REFERENCES

1 Calain, P., Roux, L. & Kolakofsky, D. Defective interfering genomes and Ebola virus persistence. *Lancet (London, England)* **388**, 659-660, doi:10.1016/s0140-6736(16)31272-7 (2016).

2 Lin, W. H., Kouyos, R. D., Adams, R. J., Grenfell, B. T. & Griffin, D. E. Prolonged persistence of measles virus RNA is characteristic of primary infection dynamics. *Proceedings of the National Academy of Sciences of the United States of America* **109**, 14989-14994, doi:10.1073/pnas.1211138109 (2012).

3 Sikkel, M. B., Quint, J. K., Mallia, P., Wedzicha, J. A. & Johnston, S. L. Respiratory syncytial virus persistence in chronic obstructive pulmonary disease. *The Pediatric infectious disease journal* **27**, S63-70, doi:10.1097/INF.0b013e3181684d67 (2008).

4 Ng, Cherie T., Snell, Laura M., Brooks, David G. & Oldstone, Michael B. A. Networking at the Level of Host Immunity: Immune Cell Interactions during Persistent Viral Infections. *Cell Host & Microbe* **13**, 652-664, doi:10.1016/j.chom.2013.05.014 (2013).

5 Strahle, L., Garcin, D. & Kolakofsky, D. Sendai virus defective-interfering genomes and the activation of interferon-beta. *Virology* **351**, 101-111(2006).

6 Sun, Y. *et al.* Immunostimulatory Defective Viral Genomes from Respiratory Syncytial Virus Promote a Strong Innate Antiviral Response during Infection in Mice and Humans. *PLoS Pathog* **11**, e1005122, doi:10.1371/journal.ppat.1005122 (2015).

7 Lopez, C. B. Defective viral genomes: critical danger signals of viral infections. *J Virol* **88**, 8720-8723, doi:10.1128/JVI.00707-14 (2014).
8 Whistler, T., Bellini, W. J. & Rota, P. A. Generation of defective interfering particles by two vaccine strains of measles virus. *Virology* **220**, 480-484 (1996).
9 Tapia, K. *et al.* Defective viral genomes arising in vivo provide critical danger signals for the triggering of lung antiviral immunity. *PLoS pathogens* **9**, e1003703, doi:10.1371/journal.ppat.1003703 (2013).
10 Yount, J. S., Kraus, T. A., Horvath, C. M., Moran, T. M. & Lopez, C. B. A novel role for viral-defective interfering particles in enhancing dendritic cell maturation. *J Immunol* **177**, 4503-4513 (2006).
11 Roux, L. & Holland, J. J. Role of defective interfering particles of Sendai virus in persistent infections. *Virology* **93**, 91-103 (1979).
12 Fernandez-Munoz, R. & Celma, M. L. Measles virus from a long-term persistently infected human T lymphoblastoid cell line, in contrast to the cytocidal parental virus, establishes an immediate persistence in the original cell line. *J Gen Virol* **73 (Pt 9)**, 2195-2202 (1992).
13 Valdovinos, M. R. & Gomez, B. Establishment of respiratory syncytial virus persistence in cell lines: association with defective interfering particles. *Intervirology* **46**, 190-198(2003).
14 Calain, P., Monroe, M. C. & Nichol, S. T. Ebola Virus Defective Interfering Particles and Persistent Infection. *Virology* **262**, 114-128 (1999).
15 Huang, A. S. & Baltimore, D. Defective viral particles and viral disease processes. *Nature* **226**, 325-327 (1970).
16 Frensing, T. *et al.* Continuous influenza virus production in cell culture shows a periodic accumulation of defective interfering particles. *PLoS One* **8**, e72288, doi:10.1371/journal.pone.0072288 (2013).
17 Roux, L., Simon, A. E. & Holland, J. J. Effects of defective interfering viruses on virus replication and pathogenesis in vitro and in vivo. *Advances in virus research* **40**, 181-211 (1991).
18 Re, G. G., Gupta, K. C. & Kingsbury, D. W. Genomic and copy-back 3' termini in Sendai virus defective interfering RNA species. *J Virol* **45**, 659-664 (1983).
19 Leppert, M., Kort, L. & Kolakofsky, D. Further characterization of Sendai virus DI-RNAs: a model for their generation. *Cell* **12**, 539-552 (1977).
20 Kirkwood, T. B. & Bangham, C. R. Cycles, chaos, and evolution in virus cultures: a model of defective interfering particles. *Proceedings of the National Academy of Sciences of the United States of America* **91**, 8685-8689 (1994).
21 Stauffer Thompson, K. A., Rempala, G. A. & Yin, J. Multiple-hit inhibition of infection by defective interfering particles. *The Journal of General Virology* **90**, 888-899, doi:10.1099/vir.0.005249-0 (2009).
22 Strahle, L., Garcin, D. & Kolakofsky, D. Sendai virus defective-interfering genomes and the activation of interferon-beta. *Virology* **351**, 101-111 (2006).
23 Bitzer, M. *et al.* Sendai virus infection induces apoptosis through activation of caspase-8 (FLICE) and caspase-3 (CPP32). *J Virol* **73**, 702-708 (1999).
24 Koyama, A. H., Irie, H., Kato, A., Nagai, Y. & Adachi, A. Virus multiplication and induction of apoptosis by Sendai virus: role of the C proteins. *Microbes and Infection* **5**, 373-378 (2003).

25 Lee, E. G. *et al.* Failure to regulate TNF-induced NF-kappaB and cell death responses in A20-deficient mice. *Science (New York, N.Y.)* **289**, 2350-2354 (2000).
26 Wang, C. Y., Mayo, M. W., Korneluk, R. G., Goeddel, D. V. & Baldwin, A. S., Jr. NF-kappaB antiapoptosis: induction of TRAF1 and TRAF2 and c-IAP1 and c-IAP2 to suppress caspase-8 activation. *Science (New York, N.Y.)* **281**, 1680-1683 (1998).
27 Liston, P. *et al.* Suppression of apoptosis in mammalian cells by NAIP and a related family of IAP genes. *Nature* **379**, 349-353, doi:10.1038/379349a0 (1996).
28 Rothe, M., Pan, M. G., Henzel, W. J., Ayres, T. M. & Goeddel, D. V. The TNFR2-TRAF signaling complex contains two novel proteins related to baculoviral inhibitor of apoptosis proteins. *Cell* **83**, 1243-1252 (1995).
29 Mercado-Lopez, X. *et al.* Highly immunostimulatory RNA derived from a Sendai virus defective viral genome. *Vaccine* **31**, 5713-5721, doi:10.1016/j.vaccine.2013.09.040 (2013).
30 Brenner, D., Blaser, H. & Mak, T. W. Regulation of tumour necrosis factor signalling: live or let die. *Nat Rev Immunol* **15**, 362-374, doi:10.1038/nri3834 (2015).
31 Dimmock, N. J. in *Viral and Other Infections of the Human Respiratory Tract* (eds Steven Myint & David Taylor-Robinson) 421-445 (Springer Netherlands, 1996).
32 Chan, Y. K. & Gack, M. U. Viral evasion of intracellular DNA and RNA sensing. *Nat Rev Microbiol* **14**, 360-373, doi:10.1038/nrmicro.2016.45 (2016).
33 Herbein, G. & O'Brien, W. A. Tumor necrosis factor (TNF)-alpha and TNF receptors in viral pathogenesis. *Proceedings of the Society for Experimental Biology and Medicine. Society for Experimental Biology and Medicine (New York, N.Y.)* **223**, 241-257 (2000).
34 Seo, S. H. & Webster, R. G. Tumor necrosis factor alpha exerts powerful anti-influenza virus effects in lung epithelial cells. *J Virol* **76**, 1071-1076 (2002).
35 Aderka, D., Holtmann, H., Toker, L., Hahn, T. & Wallach, D. Tumor necrosis factor induction by Sendai virus. *J Immunol* **136**, 2938-2942 (1986).
36 Lorence, R. M., Rood, P. A. & Kelley, K. W. Newcastle disease virus as an antineoplastic agent: induction of tumor necrosis factor-alpha and augmentation of its cytotoxicity. *Journal of the National Cancer Institute* **80**, 1305-1312 (1988).
37 Liu, L.-W., Nishikawa, T. & Kaneda, Y. An RNA Molecule Derived From Sendai Virus DI Particles Induces Antitumor Immunity and Cancer Cell-selective Apoptosis. *Mol Ther* **24**, 135-145, doi:10.1038/mt.2015.201 (2016).
38 Wertz, I. E. *et al.* De-ubiquitination and ubiquitin ligase domains of A20 downregulate NF-kappaB signalling. *Nature* **430**, 694-699, doi:10.1038/nature02794 (2004).
39 Opipari, A. W., Jr., Hu, H. M., Yabkowitz, R. & Dixit, V. M. The A20 zinc finger protein protects cells from tumor necrosis factor cytotoxicity. *The Journal of biological chemistry* **267**, 12424-12427 (1992).
40 De, A., Dainichi, T., Rathinam, C. V. & Ghosh, S. The deubiquitinase activity of A20 is dispensable for NF-kappaB signaling. *EMBO reports* **15**, 775-783, doi:10.15252/embr.201338305 (2014).
41 Greenfeld, H. *et al.* TRAF1 Coordinates Polyubiquitin Signaling to Enhance Epstein-Barr Virus LMP1-Mediated Growth and Survival Pathway Activation. *PLOS Pathogens* **11**, e1004890, doi:10.1371/journal.ppat.1004890 (2015).
42 Li, Y. *et al.* Activation of RNase L is dependent on OAS3 expression during infection with diverse human viruses. *Proceedings of the National Academy of Sciences* **113**, 2241-2246, doi:10.1073/pnas.1519657113 (2016).

43 Sun, Y. & López, C. B. Preparation of Respiratory Syncytial Virus with High or Low Content of Defective Viral Particles and Their Purification from Viral Stocks. *Bio-protocol* **6**, doi:0.21769/BioProtoc.1820 (2016).
44 Xu, J. *et al.* Identification of a Natural Viral RNA Motif That Optimizes Sensing of Viral RNA by RIG-I. *mBio* **6**, doi:10.1128/mBio.01265-15 (2015).
45 Shi, W. A Bioconductor R pipeline for analysis of RNA-seq data. (2015).
46 Bray, N. L., Pimentel, H., Melsted, P. & Pachter, L. Near-optimal probabilistic RNA-seq quantification. *Nat Biotech* **34**, 525-527, doi:10.1038/nbt.3519 (2016).
47 Soneson, C., Love, M. I. & Robinson, M. D. Differential analyses for RNA-seq: transcript-level estimates improve gene-level inferences. *F1000Research* **4**, 1521, doi:10.12688/f1000research.7563.2 (2015).
48 Law, C. W., Chen, Y., Shi, W. & Smyth, G. K. voom: Precision weights unlock linear model analysis tools for RNA-seq read counts. *Genome biology* **15**, R29, doi:10.1186/gb-2014-15-2-r29 (2014).
49 Ritchie, M. E. *et al.* limma powers differential expression analyses for RNA-sequencing and microarray studies. *Nucleic acids research* **43**, e47, doi:10.1093/nar/gkv007 (2015).
50 Huang da, W., Sherman, B. T. & Lempicki, R. A. Bioinformatics enrichment tools: paths toward the comprehensive functional analysis of large gene lists. *Nucleic acids research* **37**, 1-13, doi:10.1093/nar/gkn923 (2009).
51 Huang da, W., Sherman, B. T. & Lempicki, R. A. Systematic and integrative analysis of large gene lists using DAVID bioinformatics resources. *Nature protocols* **4**, 44-57, doi:10.1038/nprot.2008.211 (2009).
52 Subramanian, A. *et al.* Gene set enrichment analysis: A knowledge-based approach for interpreting genome-wide expression profiles. *Proceedings of the National Academy of Sciences* **102**, 15545-15550, doi:10.1073/pnas.0506580102 (2005).
53 Liao, Y., Smyth, G. K. & Shi, W. The Subread aligner: fast, accurate and scalable read mapping by seed-and-vote. *Nucleic acids research* **41**, e108, doi:10.1093/nar/gkt214 (2013).

ACKNOWLEDGMENTS

The authors wish to thank Alex Valenzuela for help with virus titrations. This work was supported by the US National Institutes of Health National Institute of Allergy and Infectious Diseases (NIH AI083284 and AI127832 to C.B.L) and The American Association of Immunologists Careers in Immunology Fellowship Program (AAI EIN 52-2317193 to C.B.L). The PennVet Imaging Core Facility instrumentation is supported by NIH S10 RR027128.

AUTHORS CONTRIBUTIONS

Conceived experiments: J.X., Y.S., and C.B.L.; Developed methodology: J.X., Y.L., D.B., A.R.; performed experiments and collected data: J.X. and Y.S.; Provided reagents and resources: G.R., Y.L., S.W., D.B., A.R.; Wrote the original draft: J.X. and C.B.L.; Supervised research activities: C.B.L.

FIGURE LEGENDS

Figure 1. Differential accumulation of SeV full-length genomes and DVGs among infected cells. (A) RNA FISH strategy. Quasar-570-labeled probes (pseudocolored red) target the 5' end of the SeV complementary genome (FL-gSeV), and Quasar-670-labeled probes (pseudocolored green) target the 3' end of the SeV complementary genome and DVGs. Polarity of genome is indicated. (B-C) RNA FISH images of A549 (B) either mock infected or infected with SeV LD alone or in the presence of pDPs (HAU = 300) for 8 h, or (C) transfected with *in vitro* transcribed (ivt) DVG or polyI:C. (D) RNA FISH images of A549 and LLC-MK2 cells infected with SeV HD. (E) RNA FISH image of lung sections from mice 5 days after SeV infection. Hoechst staining merged with individual or all channels are shown. A DVG-high cell is indicated. Images are a digital magnification from the original 20X picture. (F) Representative RNA FISH-FLOW plot of A549 cells infected for 24 h with SeV HD. Gates correspond to non-detected (ND), FL-gSeV-high cell (FL-high), intermediate (INT), and DVG-high cells. (G) Representative images of sorted cells examined under the fluorescent microscope. Top: merged fluorescent images. Bottom: fluorescent images merged with bright fields (BF). (H) Expression of SeV NP mRNA,

FL-gSeVs, and DVGs in sorted populations (n=3). (I) Representative RNA FISH-FLOW plots of A549 cells at the indicated times after SeV HD infection. Gates correspond to FL-high cell (orange), ND (blue), and DVG-high cells (green). (J) RNA FISH images corresponding to cells analyzed in (I). (K) Percentage of FL-high and DVG-high populations quantified from RNA FISH-FLOW shown in (H). One representative experiment is shown. (L) Expression of cellular *IFNB1* mRNA and SeV NP mRNA in A549 during the infection time course. RT-qPCR data are expressed as the copy number relative to the housekeeping gene *GAPDH* mRNA. *p<0.05, **p<0.01, ***p<0.001, and ****p<0.0001 by one-way (H, L) ANOVA with Bonferroni's *post hoc* test. See also Figure S1. Images were taken at a 40X (D) or 100X (B, C, G, I) magnification. Scale bar = 20μm.

Figure 2. DVG-high cells show enhanced survival during SeV infection. (A) RNA FISH images of LLC-MK2 cells infected with SeV HD or SeV LD and sub-cultured for up to 17 days. (B) Total cell numbers during the infection time course. (mean ± SEM; n=3). (C) Representative RNA FISH-FLOW analysis of LLC-MK2 cells at day 17 after mock or SeV HD infection. The percentages of ND (blue), FL-high (orange), and DVG-high (green) in the culture are indicated. (mean ± SEM; n=3). (D) Infectious virus titer in the supernatant of infected cells collected at the indicated time points. (E) A549 cells were infected with SeV HD and stained at the indicated time points using the LIVE/DEAD (L/D) Aqua viability assay followed by RNA FISH-FLOW. Representative plots are shown. ND (blue), FL-high (orange), DVG-high (green), and dead cells (white) gates are indicated. (F) Percentage of cells staining positive for L/D Aqua among each subpopulation. (mean ± SEM; n=8) (G) Percentage of cells staining positive for L/D Aqua within the total population. (mean ± SEM; n=8) (H) Representative RNA FISH-IF image of active-

caspase 3 protein (white) staining of A549 cells infected with SeV HD for 24 or 48 h. Hoechst signals were merged with either RNA FISH probes signals (left column), active-caspase 3 signal (Casp3, middle column), or all channels (right column). (I) Quantification of RNA FISH and IF staining for the apoptosis markers active-caspase 3 (left panel) and C-PARP (right panel) measured at 24 h post infection. Graphs show mean ± SEM of the percentage of FL-high, DVG-high, and other cells within the cells that stained either positive or negative for the indicated apoptotic marker, n=3-4. Stars inside column indicate significance between FL-high and DVG-high; stars between two columns indicate significance between active-caspase 3- and active-caspase3+ (or C-PARP- and C-PARP+) populations among FL-high or DVG-high sub-populations. Unless indicated, experiments were independently repeated at least 3 times. *p<0.05, **p<0.01, ***p<0.001 and ****p<0.0001 by one-way (G) or two-way (B, D, F, I) ANOVA with Bonferroni's *post hoc* test. ns=non-significant. NA = not available. See also Figure S2. Images were taken at a 20X (A) or 40X (H) magnification. Scale bar = 20μm.

Figure 3. Heterogeneous accumulation of DVG and FL-genomes during RSV infection. (A) Representative RNA FISH merged images of A549 cells infected with RSV HD at 12, 24, and 48 h after infection. (B) Representative single channel and merged images of A549 cells infected with RSV HD at 24 h post infection. Hoechst signal was merged with gRSV, DVG, or bright-field (BF) respectively. (C) Representative RNA FISH merged images of A549 cells infected with RSV HD and RSV LD at day 1, 3, 7, and 23 post infection. (D) Total cell numbers of RSV HD and LD infected cells during the infection time course. (mean ± SEM; n=3). (E) Representative merged images of RNA FISH-IF for active-caspase 3 protein (white) staining of A549 cells infected with RSV HD for 24 or 48 h. Hoechst signals were merged with either RNA

FISH probes signals (left column) or active-caspase 3 signal (Casp3, right column). (F) Percentage of active-caspase 3 positive cells within FL-high and DVG-high cells infected as in (E). Values represent mean ± SEM; n=3. *p<0.05, ***<0.001 and ****p<0.0001 by two-way ANOVA with Bonferroni's *post hoc* test. ns = non-significant. N.D = non-detectable. See also Figure S3. Images were taken at a 40X (C, E) or 100X (A, B) magnification. Scale bar = 20μm.

Figure 4. Transcriptional profiling of cells sorted based on DVG and FL-gSeV abundance identified distinct pro-survival pathways in DVG-high cells. (A) Hierarchical clustering and heatmap representation of 1800 genes differentially regulated among ND, FL-high, and DVG-high populations sorted from SeV HD-infected A549 cells at 24 h post infection. Color based on row Z-score. Three clusters of distinctly upregulated genes in each of the sorted sub-populations are indicated. (B) Bubble chart showing Gene Ontology (GO) enrichment analysis. Bubble size indicates the number of genes associated with each term. Bubble color intensity indicates fold enrichment of GO terms overrepresented in that cluster of genes. Pathways upregulated in each cluster were color-coded as blue (Cluster 1), green (Cluster 2) and orange (Cluster 3). (C) GSEA enrichment plot for four selected pathways differentially regulated in the DVG-high cells compared with others. Normalized enrichment scores (NES) and false discovery rate (FDR) are indicated. (D) Selected genes from each GSEA signature panel shown in (C). Average fold change (FC) between DVG-high and FL-high cells is shown. N = ND, D = DVG-high, and F = FL-high in the mini-heatmaps shown in the left side of each graph. See also Figure S4.

Figure 5. Distinct TNF pathways determine the cells fate during virus infection. (A-C) A549 CRISPR control (CTRL), IFNAR1 KO and MAVS KO cells mock-infected or infected with SeV

HD for 24 or 48 h. (A) Merged representative RNA FISH-IF images of active caspase-3 positive staining. Magnification: 40X. Scale bar =20 μm. (B) Percentage of active caspase-3 positive cells within each infected culture. (mean ± SEM; n=8). (C) Percentage of active caspase-3 positive cells within the FL-high and DVG-high populations of each culture. (mean ± SEM; n=8). (D) TNFα in the supernatant of A549 CTRL, IFNAR1 KO, and MAVS KO cells mock infected or infected with SeV for 24 h. One representative experiment is shown, bar = mean ± SEM of technical triplicate. (E) Percentage of active-caspase 3 positive MAVS KO cells infected with SeV HD for 16 h and either left un-treated (UT), treated with recombinant IFN-beta (IFNβ, 100U), or treated with recombinant TNFα (10ng/ml) for 8 h. (mean ± SEM; n=3). (F-G) A549 cells were infected with SeV HD and incubated with control IgG antibody or antibodies against TNFα, TNFR1 and TNFR2 (anti-TNF Combo). (F) Percentage of apoptotic A549 cells from the total population. (mean ± SEM; n=4). (G) Percentage active-caspase 3 positive cells within FL-high and DVG-high cells. (mean ± SEM; n=4). (H-I) MAVSKO A549 cells were infected with SeV HD for 16 h and then incubated with recombinant TNFα at 0,0.05,1 and 10 ng/ml for 8 h. (H). Percentage of active-caspase 3 positive cells among total cells (n=3-6). (I). Percentage of active-caspase 3 positive staining cells within FL-high and DVG-high cells. Values represent mean ± SEM of fold change over UT at each TNFα dosage; n=3. *p<0.05, **p<0.01, ***p<0.001, and ****<0.0001 by one-way (E, H) or two-way (B-C, F, G, I) ANOVA with Bonferroni's *post hoc* test. Ns = non-significant. ND = non-detected. See also Figure S5.

Figure 6. The survival response of DVG-high cells is regulated by MAVS signaling. (A-B) SeV HD infected A549 cells treated with either control-IgG, TNFR1 or TNFR2 neutralizing antibodies. (A) Percentage of active-caspase 3 positive cells within the total cultures. (mean ±

SEM; n=4). (B) Percentage of active-caspase 3 positive cells within FL-high and DVG-high cells in each condition. (mean ± SEM; n=4). (C-D) A549 cells transfected with either control siRNA (si-Control) or *TRAF1* siRNA (si-*TRAF1*) followed by SeV HD infection for 24 h. (C) Percentage of apoptotic cells within the total cell cultures. (mean ± SEM; n=3). (D) Percentage of active-caspase 3 positive cells within FL-high and DVG-high cells in each condition. (mean ± SEM; n=3). (E and F) A549 CTRL and MAVS KO cells infected with SeV LD and HD (MOI=1.5 $TCID_{50}$/cell) for 24 h. (E) Expression of surface TNFR2 was quantified by flow cytometry (n=4) and (F) expression of cellular *TRAF1*, *BIRC3*, and *TNFAIP3* (A20) mRNA by RT-qPCR. Data are expressed as mean ± SEM copy number relative to the housekeeping gene *GAPDH*; (n=4). *p<0.05, **p<0.01, ***p<0.001, and ****<0.0001 by one-way (A) or two-way (B, D-F) ANOVA with Bonferroni's *post hoc* test, or unpaired t-test (C). ns = non-significant. (G) Schematic representation of proposed model. DVGs-high cells engage a MAVS-dependent anti-viral pathway that drives the antiviral response and the apoptosis of neighboring cells through the production of TNF (denoted 1), while protecting the cytokine-producing cell from death through a TNFR2/TRAF1 mediated mechanism (denoted 2). See also Figure S6.

Figure 1

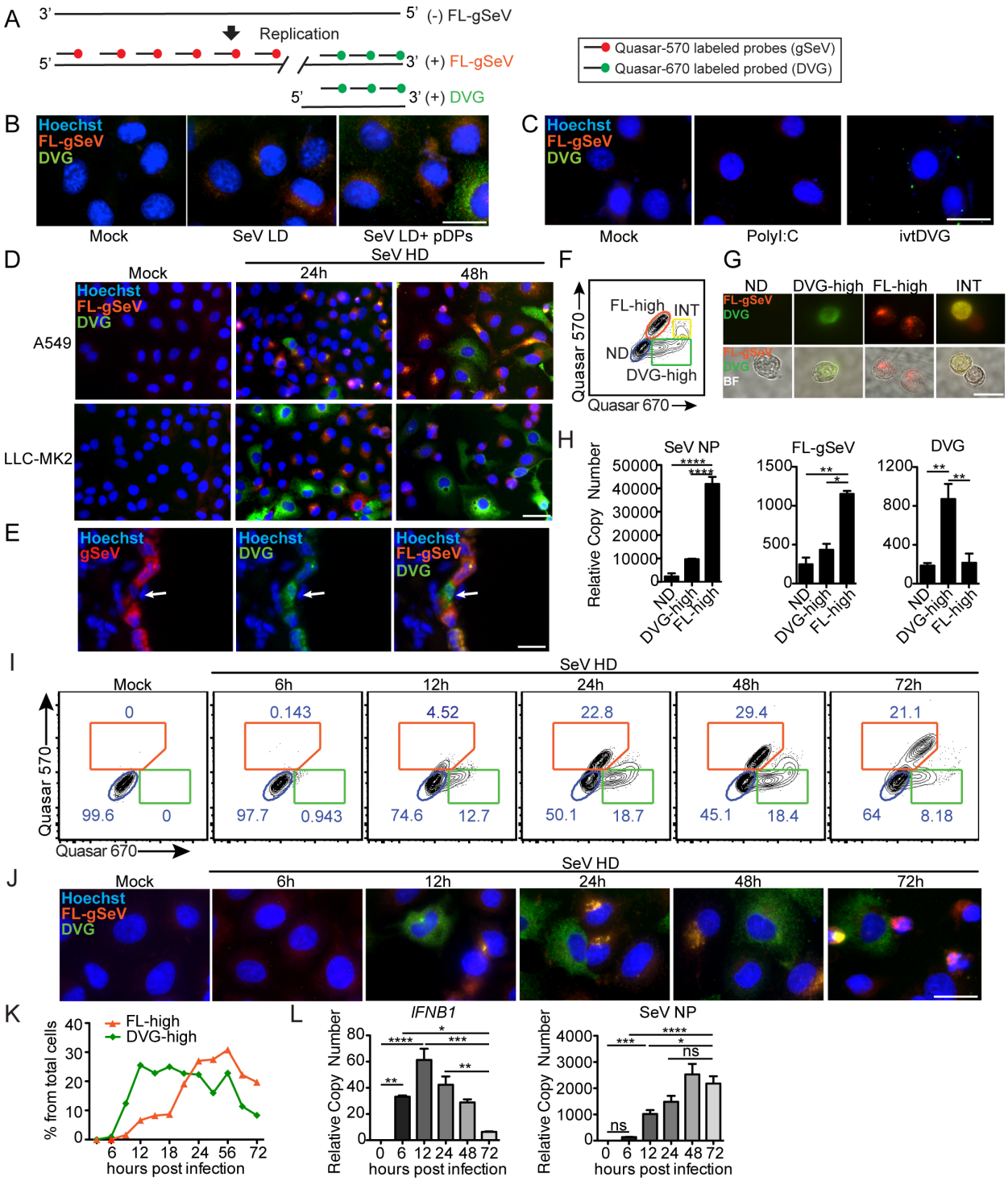
A
3'
5' (-) FL-gSeV
Replication
5'
3' (+) FL-gSeV
5'
3' (+) DVG
Quasar-570 labeled probes (gSeV)
Quasar-670 labeled probed (DVG)
B
Hoechst
FL-gSeV
DVG
Mock
SeV LD
SeV LD+ pDPs
C
Hoechst
FL-gSeV
DVG
Mock
PolyI:C
ivtDVG
D
SeV HD
Mock
24h
48h
A549
LLC-MK2
Hoechst
FL-gSeV
DVG
E
Hoechst
gSeV
Hoechst
DVG
Hoechst
FL-gSeV
DVG
F
FL-high
INT
ND
DVG-high
Quasar 570
Quasar 670
G
ND
DVG-high
FL-high
INT
FL-gSeV
DVG
BF
H
SeV NP
FL-gSeV
DVG
Relative Copy Number
ND
DVG-high
FL-high
I
SeV HD
Mock
6h
12h
24h
48h
72h
Quasar 570
Quasar 670
0
99.6
0
0.143
97.7
0.943
4.52
74.6
12.7
22.8
50.1
18.7
29.4
45.1
18.4
21.1
64
8.18
J
SeV HD
Mock
6h
12h
24h
48h
72h
Hoechst
FL-gSeV
DVG
K
FL-high
DVG-high
% from total cells
hours post infection
L
IFNB1
SeV NP
Relative Copy Number
hours post infection

Figure 2

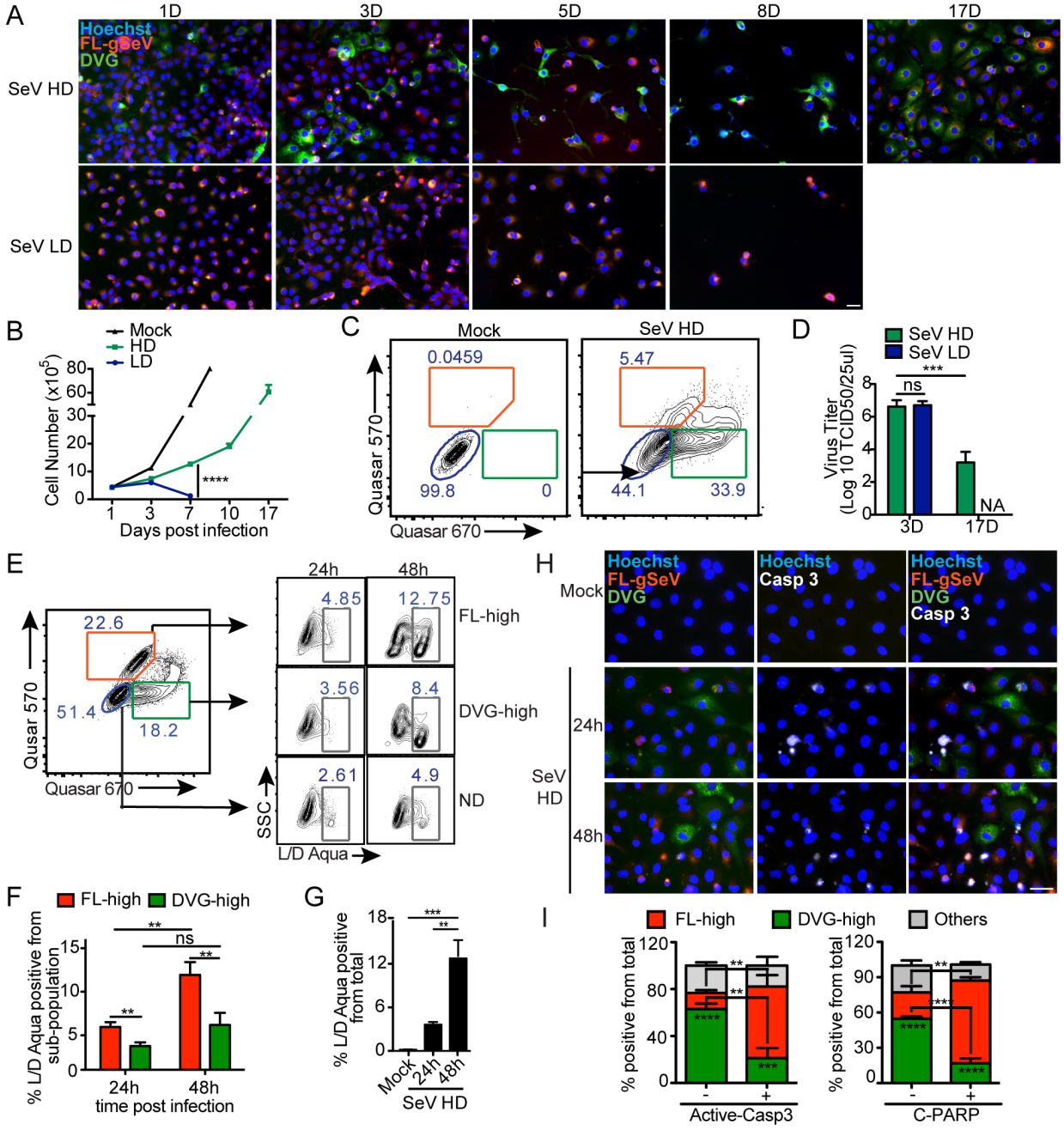
A
1D
3D
5D
8D
17D
Hoechst
FL-gSeV
DVG
SeV HD
SeV LD
B
Mock
HD
LD
Cell Number (x10^5)
Days post infection
****
C
Mock
SeV HD
0.0459
99.8
0
5.47
44.1
33.9
Quasar 570
Quasar 670
D
SeV HD
SeV LD
Virus Titer (Log 10 TCID50/25ul)
***
ns
NA
3D
17D
E
22.6
51.4
18.2
Quasar 570
Quasar 670
24h
48h
4.85
12.75
FL-high
3.56
8.4
DVG-high
2.61
4.9
ND
SSC
L/D Aqua
H
Mock
Hoechst
FL-gSeV
DVG
Hoechst
Casp 3
Hoechst
FL-gSeV
DVG
Casp 3
SeV HD
24h
48h
F
FL-high
DVG-high
% L/D Aqua positive from sub-population
**
ns
24h
48h
time post infection
G
% L/D Aqua positive from total
***
**
Mock
24h
48h
SeV HD
I
FL-high
DVG-high
Others
% positive from total
Active-Casp3
C-PARP

Figure 3

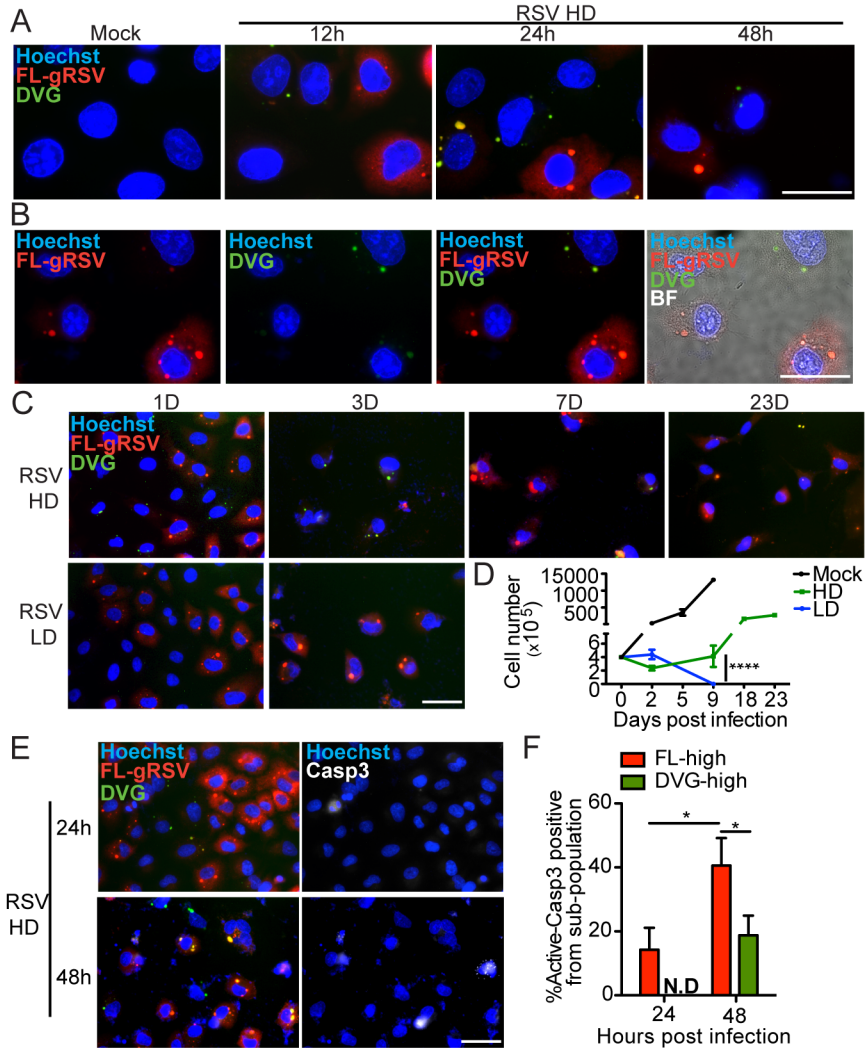
A
Mock
RSV HD
12h
24h
48h
Hoechst
FL-gRSV
DVG
B
Hoechst
FL-gRSV
Hoechst
DVG
Hoechst
FL-gRSV
DVG
Hoechst
FL-gRSV
DVG
BF
C
1D
3D
7D
23D
Hoechst
FL-gRSV
DVG
RSV
HD
RSV
LD
D
Cell number
(x10^5)
15000
1000
500
6
4
2
0
****
0 2 5 9 18 23
Days post infection
Mock
HD
LD
E
Hoechst
FL-gRSV
DVG
Hoechst
Casp3
24h
48h
RSV
HD
F
FL-high
DVG-high
%Active-Casp3 positive
from sub-population
60
40
20
0
*
*
N.D
24
48
Hours post infection

Figure 4

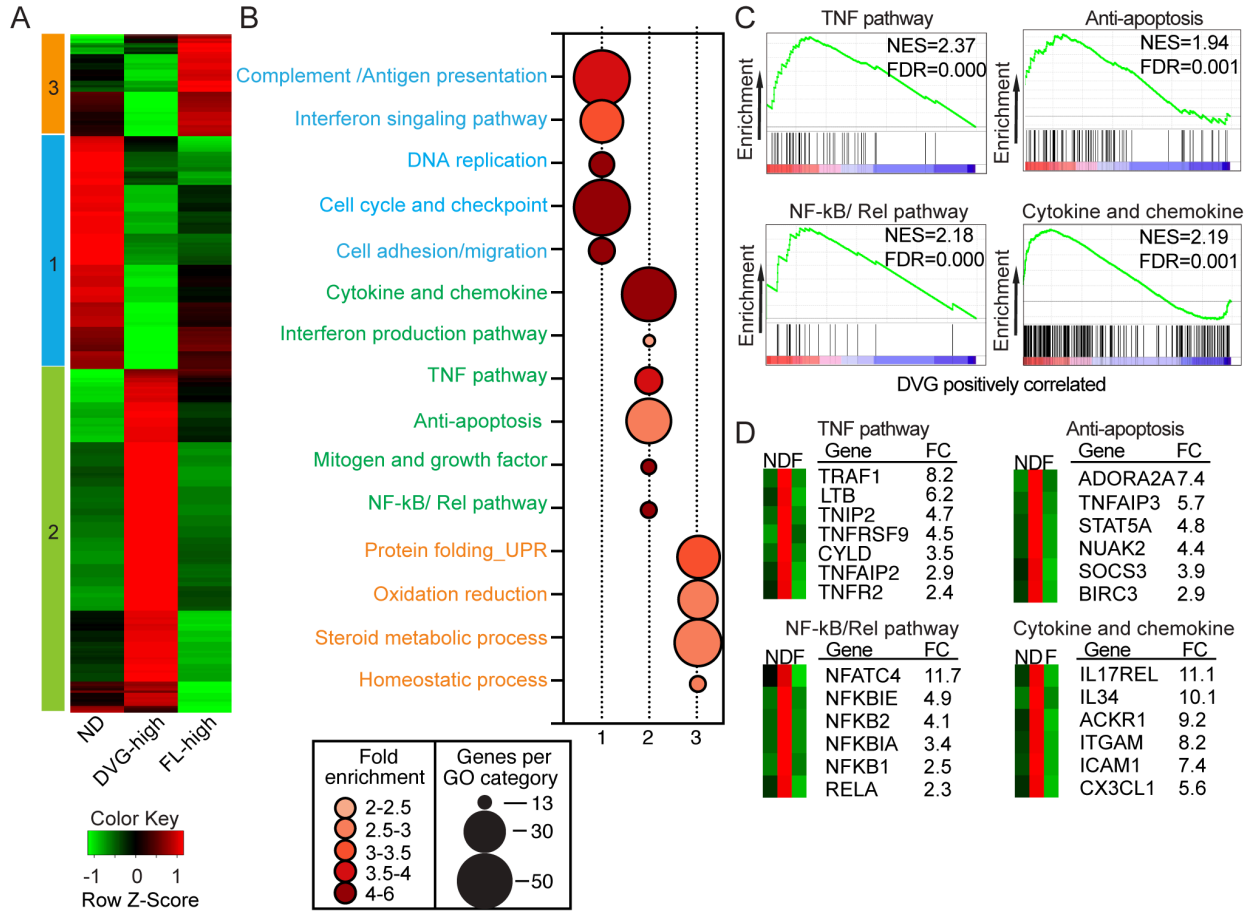
A
3
1
2
ND
DVG-high
FL-high
Color Key
-1 0 1
Row Z-Score
B
Complement /Antigen presentation
Interferon singaling pathway
DNA replication
Cell cycle and checkpoint
Cell adhesion/migration
Cytokine and chemokine
Interferon production pathway
TNF pathway
Anti-apoptosis
Mitogen and growth factor
NF-kB/ Rel pathway
Protein folding_UPR
Oxidation reduction
Steroid metabolic process
Homeostatic process
1 2 3
Fold enrichment
2-2.5
2.5-3
3-3.5
3.5-4
4-6
Genes per GO category
13
30
50
C
TNF pathway
NES=2.37
FDR=0.000
Anti-apoptosis
NES=1.94
FDR=0.001
NF-kB/ Rel pathway
NES=2.18
FDR=0.000
Cytokine and chemokine
NES=2.19
FDR=0.001
Enrichment
DVG positively correlated
D
TNF pathway
NDF
Gene FC
TRAF1 8.2
LTB 6.2
TNIP2 4.7
TNFRSF9 4.5
CYLD 3.5
TNFAIP2 2.9
TNFR2 2.4
Anti-apoptosis
NDF
Gene FC
ADORA2A 7.4
TNFAIP3 5.7
STAT5A 4.8
NUAK2 4.4
SOCS3 3.9
BIRC3 2.9
NF-kB/Rel pathway
NDF
Gene FC
NFATC4 11.7
NFKBIE 4.9
NFKB2 4.1
NFKBIA 3.4
NFKB1 2.5
RELA 2.3
Cytokine and chemokine
NDF
Gene FC
IL17REL 11.1
IL34 10.1
ACKR1 9.2
ITGAM 8.2
ICAM1 7.4
CX3CL1 5.6

Figure 5

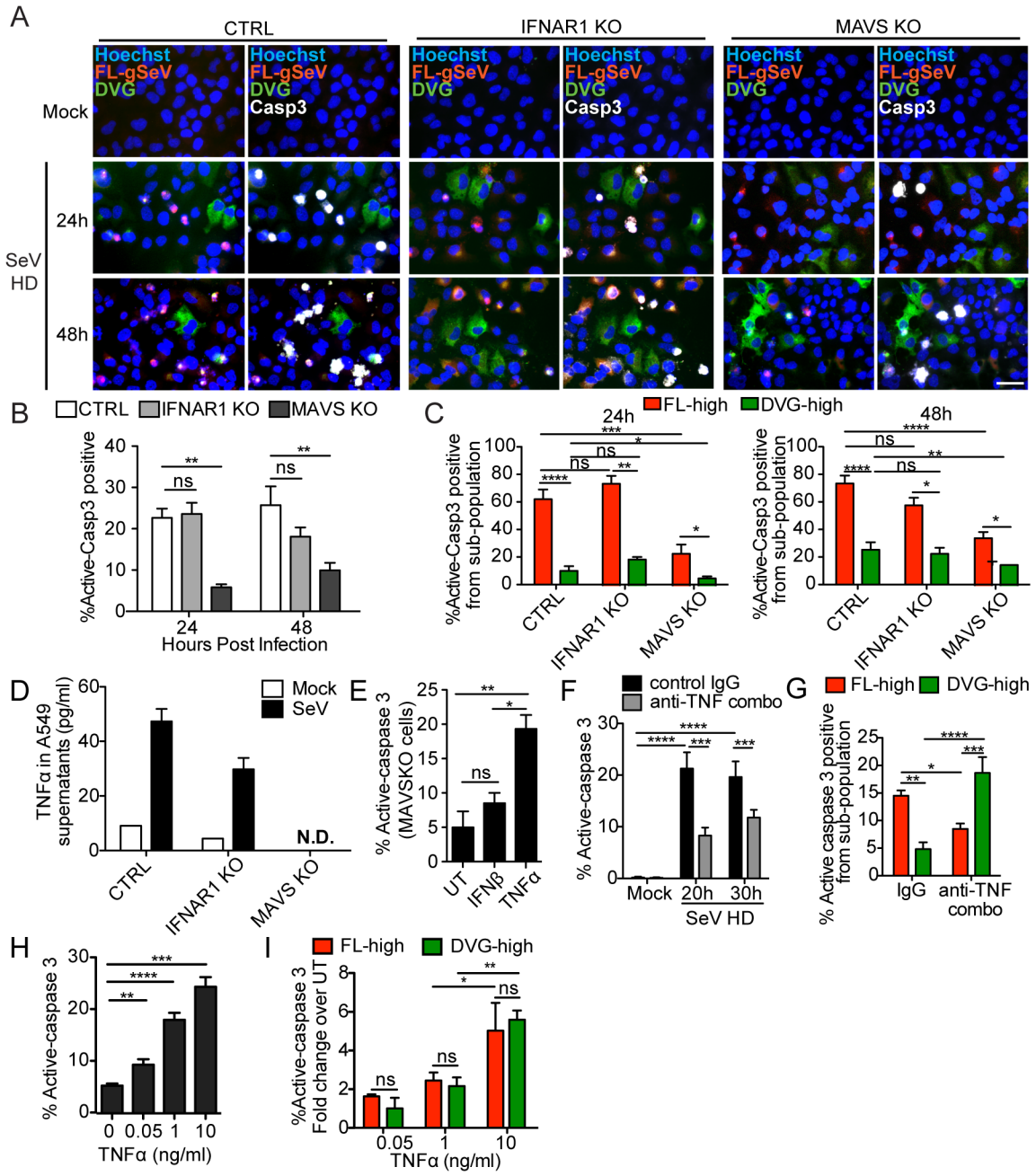
A
CTRL
IFNAR1 KO
MAVS KO
Hoechst
FL-gSeV
DVG
Casp3
Mock
SeV HD
24h
48h
B
CTRL
IFNAR1 KO
MAVS KO
%Active-Casp3 positive
Hours Post Infection
C
FL-high
DVG-high
%Active-Casp3 positive from sub-population
D
Mock
SeV
TNFα in A549 supernatants (pg/ml)
N.D.
E
% Active-caspase 3 (MAVSKO cells)
UT
IFNβ
TNFα
F
control IgG
anti-TNF combo
% Active-caspase 3
SeV HD
G
% Active caspase 3 positive from sub-population
IgG
anti-TNF combo
H
% Active-caspase 3
TNFα (ng/ml)
I
%Active-caspase 3 Fold change over UT
TNFα (ng/ml)

Figure 6

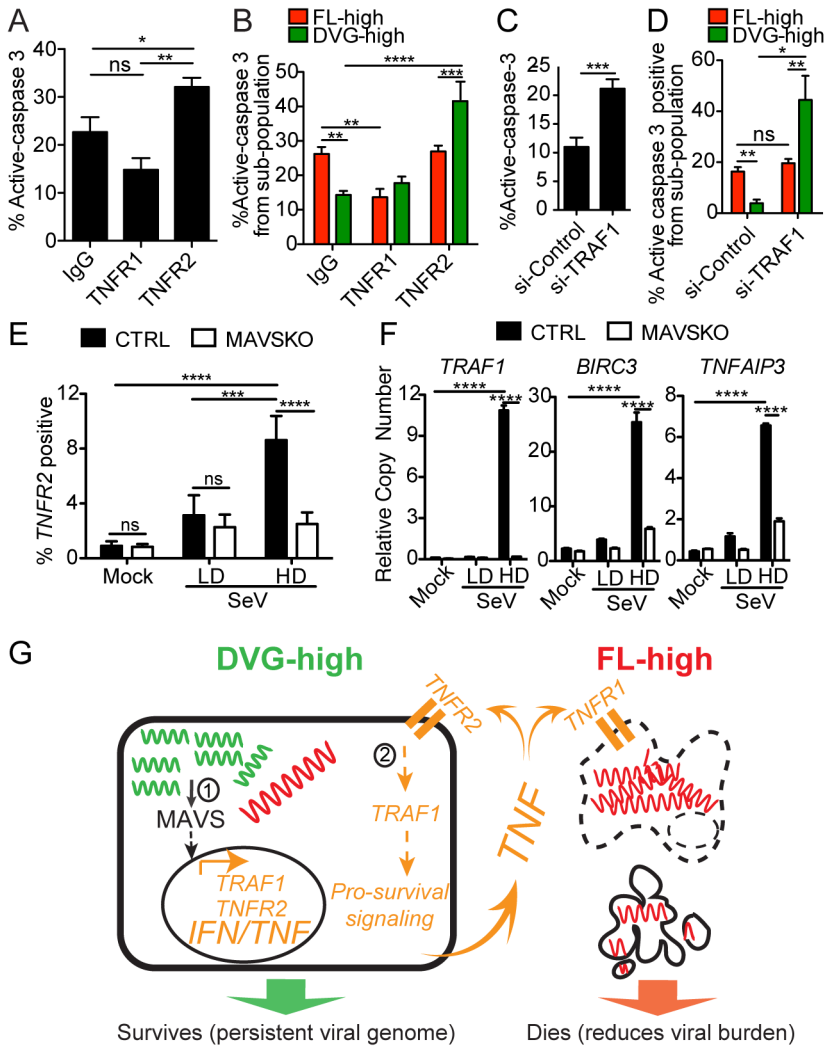
A
% Active-caspase 3
IgG
TNFR1
TNFR2
B
FL-high
DVG-high
%Active-caspase 3 from sub-population
C
%Active-caspase-3
si-Control
si-TRAF1
D
% Active caspase 3 positive from sub-population
E
CTRL
MAVSKO
% TNFR2 positive
Mock
LD
HD
SeV
F
TRAF1
BIRC3
TNFAIP3
Relative Copy Number
G
DVG-high
FL-high
TNFR2
TNFR1
MAVS
TRAF1
TRAF1
TNFR2
IFN/TNF
Pro-survival signaling
TNF
Survives (persistent viral genome)
Dies (reduces viral burden)